Check for updates

Structure and flow conditions through a colloidal packed bed formed under flow and confinement†

N. Delouche,[a] B. Dersoir,[a] A. B. Schofield [ID][b] and H. Tabuteau [ID] *[a]

When a colloidal suspension flows in a constriction, particles deposit and are able to clog it entirely, this fouling process being followed by the accumulation of particles. The knowledge of the dynamics of formation of such a dense particle assembly behind the clog head and its structural features is of primary importance in many industrial and environmental processes and especially during filtration. While most studies concentrate on the conditions under which pore clogging occurs, *i.e.*, the pore narrowing up to its complete obstruction, this paper focuses on the accumulation of particles that follows pore obstruction. We determine the relative contribution of the confinement dimensions, the ionic strength and the flow conditions on the permeability and particle volume fraction of the resultant accumulation. In high confinement the irreversible deposition of particles on the channel surfaces controls the structure of the accumulation and the flow through it, irrespective of the other conditions, leading to a Darcy flow. Finally, we show that contrarily to the clog head, in which there is cohesion between particles, those in the subsequent accumulation are held together by the fluid and form a dense suspension of repulsive hard spheres.

Introduction

The progressive formation of dense colloidal suspensions or colloidal gels near a surface/interface occurs in various natural and industrial processes. Colloidal particles sediment to the bottom of the ocean or river bed, they can also be driven by an evaporative flux near the contact line of a drying drop and form the so-called coffee ring pattern[1] or they accumulate on top of a filtration membrane in a filter cake.[2,3] In all these examples the structure of the accumulated colloidal suspension results from the coupling between the advective flow, the confinement dimensions and the interparticle forces. Most of the previous studies into this type of accumulation have focused on the effect of the confinement on the evolution of the structural features of the dense particle assembly, with a negligible analysis of the effect of the flow. For purely hard sphere like particles, dense deposits with an ordered structure are formed near the contact line of a drying drop, irrespective of the evaporation rate,[4,5] or at the bottom of a tube under gravity, or ultracentrifugation conditions using 100 to 1000g.[6] Confining systems like colloidal suspensions, with $0.19 < \phi < 0.52$, ϕ

being the particle volume fraction, leads to a lower mobility of particles, similar to the glassy dynamics observed for higher ϕ in bulk samples either for hard sphere[7–10] or weakly attractive suspensions.[11] These reports also show that the roughness of the confining walls affects the local structure and further slows down particle dynamics.[8,12–15] For monodisperse hard sphere colloids if $\phi \geq 0.48$, they can form a crystal. Pieransky *et al.*[16] observed the successive structural transitions of such crystals under confinement as long as the distance between the two confining plates is not greater than 10D, D being the particle diameter. Particles are alternatively arranged in a hexagonal and a square lattice as the separation between the two plates increases. It has been shown by Pansu *et al.*[17] and later by Palberg *et al.*[18] that there are intermediate structures between the hexagonal and the square ones, which allow particles to pack more efficiently if a slight compression or a shear is exerted on the particle layers. The buckling of the layers leads to the formation of prisms periodically separated by stacking fault defects.[19]

Dense packing of hard spheres can also be progressively formed under flow. Ortiz *et al.*[20] studied the formation of a deposit of polystyrene particles ($D = 0.5$ μm), transported by a fluid flow, over a porous obstacle in very high confinement (channel height H is around 0.9 μm and $H/D = 1.8$), for low Péclet number ($0.3 < Pe < 30$). They showed that the deposit behaved as a dense repulsive glass with the particles being held together on the porous obstacle by the flow. By varying periodically the flow rate they also showed that the deposit was slightly

[a] *Univ Rennes, CNRS, IPR (Institut de Physique de Rennes)-UMR 6251, F-35000 Rennes, France. E-mail: herve.tabuteau@univ-rennes1.fr*

[b] *School of Physics and Astronomy, The University of Edinburgh, The James Clerk Maxwell Building, The King's Buildings, Mayfield Road, Edinburgh, UK*

† Electronic supplementary information (ESI) available. See DOI: **https://doi.org/10.1039/d2sm00419d**

compressible.[21,22] The structural features of particle accumulations are different when there is an attraction either between particles or between particles and the walls of the channel. For instance, the accumulation has a tenuous gel-like structure when there is a net attraction between particles.[23] More generally, the structure of the accumulation is either compact or tenuous depending on the DLVO interparticle potentials and the hydrodynamic conditions as shown by Saint Vincent et al.[24] They performed experiments similar to that of Ortiz et al.[20] but in a less confined situation ($H/D = 4$), in which they accumulated particles on a single pore. By systematically varying the ionic strength, I, and the Pe number they observed various shapes of deposit. For low I, the particle accumulation formed at the entrance of pore is labile and has a limited growth, irrespective of the flow conditions. Larger and cohesive accumulations are observed when I increases such that particle surface charges are completely screened.

Formation of a dense particle assembly under confinement also takes place just after the clogging of a single constriction or of the main flow paths of confined media like filters, soils, rocks, microfluidic devices or even the blood circulation system. Clogging mechanisms can be different depending on the nature, the geometrical features and the surface properties of the suspending (bio)-particles.[25–27] To gain a deeper understanding of this multiscale, multi-parameter and catastrophic phenomenon most of the previous works have studied it inside a single constriction or pore. In such a case, the clogging mechanisms mainly depend on the size ratio W/D, with W the constriction size, and to a lesser extent on the particle volume fraction of the flowing suspension, ϕ. Rigid particles are directly sieved when their diameter is larger than the dimension of the constriction[28,29] while for deformable particles like proteins[27] and microgels[30,31] sieving only occurs so long as the pressure in the system is low enough that these type of particles cannot rearrange and get pushed through the constriction. For particles smaller than the constriction size, several particles are always involved in the obstruction process. For small size ratios, $W/D < 3$, when several particles, over a wide range of diameter from 200 nm up 100 μm, are about to flow inside a constriction they form a bridge at its entrance,[32–36] a process that does not depend on the particle volume fraction of the flowing suspension. Arch formation occurs very frequently for high ϕ values,[35–37] between 0.2 and 0.6 while it is rarer for low ϕ values,[33,38] between 10^{-4} and 10^{-2}. While the dynamics of arch formation with colloidal particles has never been observed experimentally, several studies have clearly shown that pore clogging for $10^{-5} < \phi < 10^{-2}$ is more often a progressive process, particles accumulating one by one in the pore, up to its complete obstruction.[39–44] All the above mentioned studies are directly related to the reduction of the cross section of the pore up to the complete stoppage of particle transport and they do not consider the particle accumulation that follows this pore blockage. Very few studies have simultaneously considered these two parts of the clogging process and the relationship between them. Mokrane et al.[45] worked on the accumulation of particles upstream of the entrance of a 2D model filter in a very

low confinement ($H/D = 18$). The filtering part of the channel, i.e., the narrowest part, is first clogged at its entrance by a progressive accumulation of a few particles. Thereafter, in the reservoir zone just upstream of the pores, particles are either stuck on the channel surfaces, or they accumulate in the bulk, forming a dense assembly of repulsive spheres, maintained together by the fluid pressure. Mokrane et al. determined the structural features of the monolayer in contact with one of the horizontal pore surface and from these measurements they showed that particles form an amorphous and more porous structure near the pore entrance while further away there is a crystalline order, with a lower porosity. However, we do not know what the structure of the particles are in the bulk and if the evolution of this structure is influenced by the behavior of the particles in the monolayers close to the pore surface. Sauret et al. clogged pores with large contaminants leading to the accumulation of 2 μm particles in a rectangular channel whose width, W, and height, H, are respectively equal to 40 and 14 μm.[46] They showed that after the initial sieving event the clog growth increases the hydraulic resistance of the channel and thus leads to a flow decline, the structure of the accumulation being amorphous. Using the temporal evolution of the length of the accumulation they determined the clog permeability corresponding to this flow decline with the Carman–Kozeny equation. They found that the value of the particle volume fraction of the accumulation, also called ϕ thereafter, is somewhat high and around 0.7. Another study conducted similar experiments in a more confined situation using a channel with an almost squared cross section channel ($W = 9$ μm and $H = 11$ μm) and 1.8 μm particles.[44] Thanks to the internal structure of the accumulation at the particle level, obtained using confocal microscopy, they found a much lower value of ϕ, around 0.32. They showed that there is an heterogeneous flow inside the clog corresponding to a Darcy-like flow with most of the flow passing through a preferential path that connects wide void zones inside the accumulation. Overall, the relationship between ϕ, the degree of confinement and the flow within an accumulation of colloidal particles remains unclear despite the fundamental and practical implications of knowing this.

In this paper, we consider the evolution of the structural features of a dense colloidal suspension in confined situations that is formed by particle accumulation in a channel upstream of an obstructed pore. We determine the permeation flow through the particle accumulation and try to see if there is any relationship between the flow variations inside this accumulation and its structural features including the particle volume fraction. We determine the permeability in situ of the growing accumulation from its length and the variations of the fluid velocity. In addition, we look at the effect of the confinement, ionic strength and flow conditions on both the structural features of the accumulations and the flow through them. We show that the degree of confinement and the shape of the channel cross section have the greatest impact on the mean structure of the clog. Under high confinement the structure of the clog is always heterogeneous and rather porous with a low ϕ, around 0.3–0.35, while for slight modifications of the area of the channel cross

section ϕ is closer to 0.5–0.6. The influence of the particle deposited on the channel surfaces and to a lesser extent the nature of the objects (shape and size) that accumulate are put forward to explain the variations in ϕ. Contrary to large and wide porous media composed of spherical particles, for which there is a direct relationship between ϕ and the flow conditions inside the porous structure, the Carman–Kozeny relationship cannot be used to predict the permeability of dense colloidal suspensions in high confinement since wall effects are not negligible. The flow within the particle accumulation is heterogeneous and mostly relies on a few preferential paths rather than exploring most the pore space between the particles. Nevertheless, we found that the permeability of the particle accumulation is constant, which corresponds to a Darcy flow. Finally, by performing de-clogging experiments in the most confined situation, we show that the presence of particle monolayers on the walls of the channel with a high ϕ leads to the formation of a cohesive zone inside the accumulation, due to the presence of arches across the channel height.

Materials and methods

Details about the lithography, the pore geometry and imaging techniques used in this work can be found in previous papers.[39,40,44] Briefly, we employ a device with two long reservoirs followed by a constriction/pore in which the progressive obstruction by particle deposition takes place (Fig. 1). The different parts of channels are defined with a height H and a width W. Fluorescent PMMA particles with diameters D = 1.8 and 4.0 ± 0.1 µm were synthetized by following the methods described in the paper of Shen *et al.*,[47] while PS particles coated by a polyelectrolyte brush were synthetized according to the protocol described in ref. 41 and 48. PS particles with various diameters (1, 1.5, 1.8, 2, 3, 4 and 6 µm) were supplied by Microparticle (Gmbh, Berlin) or Life Technology (USA). We use a dilute suspension of these particles with a particle volume fraction of 5×10^{-3}, which enables us to track all the particles
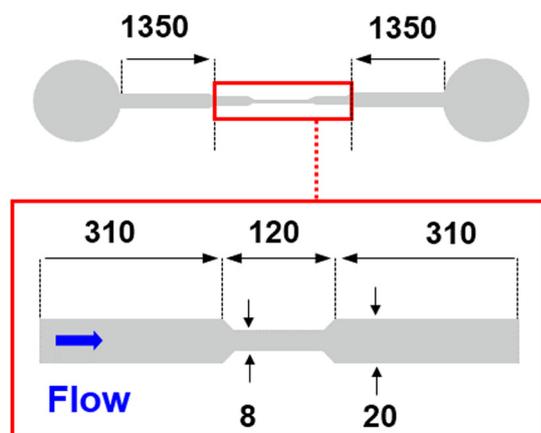

Fig. 1 Geometry of the microfluidic channel. The zoom highlights the constriction zone where the colloidal clog is formed behind which particles accumulate. All dimensions are µm.

that flow through the channel and determine their shape and velocity. In the most confined situation H/D is equal to 3, while for the less confined case H/D = 12.9 and $W \geq H$, irrespective of the confinement. We determine the local particle volume fraction, ϕ, every 13 µm along the accumulation. Over this distance, we count the number of particles that accumulate over time, irrespective of the particle diameter, and calculate the ratio of the volume of all the particles over the volume of the section of the channel. A distance of 13 µm is large enough to minimize the error in the ϕ values, this error being equal to 0.05. At the same time, this distance is small enough to monitor the variation of ϕ for accumulations with a total length of around 200–250 µm. We use this local measurement method for Fig. 2(a) while for all the other figures we use a cumulated volume fraction. For this later method, we still count the number of particles for slices of width $7D$ but for each new slice we calculate ϕ on the overall accumulation length, L_{acc}, rather than on the width of the last slice. We also used high speed confocal microscopy (VT-Infinity III) to get the positions of immobile particles within the channel for the determination of ϕ for the 1.8 and 4 µm fluorescent PMMA particles. We work with an applied pressure across the channel at a low Reynolds number, Re $< 10^{-4}$, and with a wide range of Péclet numbers ($1.6 \times 10^{2} <$ Pe $< 7 \times 10^{5}$).

We quantify the compaction of the particle accumulation using the image analysis program developed by Lüken *et al.*[49] which is able to detect individual and collective motions of particles inside a dense particle assembly such as is seen in a colloidal filter cake. In our case, this image analysis also allows us to detect rearrangements at the particle level, irrespective of the size or number of particles involved in such an event (Fig. S1, ESI†). From this analysis we determine the length and the width of the surface over which there is a rearrangement and the average number of particles that are involved. De-clogging experiments are performed using a decreasing pressure ramp followed by a constant pressure step that lasts around 2 minutes. For all the experiments we use the same ramp, decreasing the pressure from its initial value by 0.05 mbar every 10 seconds. We stop decreasing the pressure either when a significant part of the accumulation is removed, at least a few tens of particles, or when the total pressure variation reaches a maximum of 20 mbar. For all the experiments we have to reverse the flow direction to observe a de-clogging event. However, since we use a pressure ramp with a small slope we observe less catastrophic de-clogging events than seen by Mokrane *et al.* since they rapidly switch the pressure to zero.[45] Note, that in their case the confinement along the height of the channel is much less important since H/D = 18, and thus the role of the channel surface is really minimal compared to our configuration. Our de-clogging protocol is also different from that of Dincau *et al.* who also reverse the flow direction but in a periodic manner.[50] The use of pulsatile flow proves to be helpful in delaying pore clogging by successive particle depositions for confinements comparable to those used here, but its impact on the subsequent accumulation has not yet been studied.
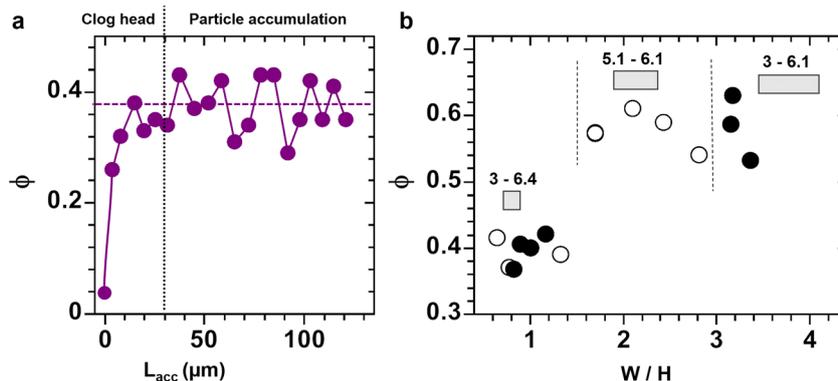
Fig. 2 (a) Variation of ϕ along the clog length for 2 μm PS inside a constriction with a cross section of 6.9 × 8 μm. The complete obstruction takes place over the first 30 μm followed by the particle accumulation, the two steps being separated by the vertical dotted line. (b) Evolution of ϕ with the ratio of the width over the height of the channel. Hollow and full circles correspond to particles stabilized by a polymer brush and surface charge, respectively. The mean cross section of the channel is drawn for three zones separated by two dashed lines. For each zone we indicate the range of the height of the channels scaled by the particle diameter, which is between 1.5 and 4 μm.

Results

1 Evolution of the particle volume fraction inside the clog formed in various confinements

The clogging dynamics of a pore is composed of two consecutive steps, regardless of the dimensions of the pore and the position of the head of the clog inside the pore.[44] The pore is first progressively fouled by particle deposition during which the mean particle volume fraction, ϕ (see Methods), increases with the length of the clog, over a few tens of microns, depending on the cross section of the pore. This process continues until there is complete obstruction of the pore and corresponds to the formation of what we call the clog head (Fig. 2(a)). In this article, we focus on the subsequent step during which particles accumulate at the rear of the clog head. We observed that ϕ always fluctuates around a mean value along the clog length, whatever the confinement used (Fig. 2(a)) as shown in Delouche et al.[44] There are two ranges of ϕ depending on the ratio of the width over the height of the channel, W/H, irrespective of the particle diameter (Fig. 2(b)). When the cross section is square, the volume fractions are low, $0.35 < \phi < 0.45$. When the cross sections become rectangular, for channels wider than high, we obtain higher volume fractions, $0.5 < \phi < 0.63$, irrespective of the type of particle stabilization, (steric or surface charges).

For nearly squared cross sections, i.e. for W/H around one, the range of values of ϕ is too high to consider that the particle accumulation has the structure of a colloidal gel formed only by diffusion[51–53] or under flow during clogging of the pore.[34] Indeed, for comparable particle sizes to those used here, the mean volume fraction for colloidal gels is closer to 0.05–0.15, which is much smaller than the 0.3–0.4 measured here. Therefore, the structure of the particle accumulation cannot be explained either by diffusion- and reaction-limited cluster aggregation theories (DLCA and RLCA, respectively). Here the structure of the particle accumulation is mostly driven by the flow. For the strongest confinement along z ($H/D = 3$ and $W/D = 4$) flowing particles are first captured by the channel surfaces and form

monolayers with a disordered structure full of void zones all around the channel.[40] The deposition of new particles on the surfaces is highly dependent on the presence of those already deposited. Indeed, for such a high confinement, a particle in contact with one surface of the channel locally reduces its cross section and thus acts as a local constriction, which favors the deposition of other particles that flow in its vicinity.[40,43] Further on in the accumulation process, a few particles are found in the middle of the channel that are just blocked between the monolayers in contact with the channel surface.[40] Therefore, the low ϕ value around 0.4 is mainly due the partial covering of the surfaces of the channel. For the lowest confinement ($H/D = 6.4$ and $W/D = 5$) flowing particles are captured by the channel walls and form up to three layers with a very heterogeneous structure and wide void zones.[44] This irregular repartition of particles on the channel surface is also responsible for the sudden and large fluctuations of ϕ along the accumulation length, up to 30% of the mean value, as the clog grows (Fig. 2(a)). There is also significant variations of ϕ between each clogging experiment since the dynamics of obstruction of each channel is unique, in particular the spatial repartition of the single particles and aggregates on the pore surface.[40,44] We observe that there are small rearrangements as particle accumulate, these events being located only at the accumulation front and involving between one and two particles, (Fig. S2, ESI†). There may also be displacements of other particles not in contact with the bottom pore surface which are not detectable by our image analysis. This very limited compaction indicates that almost all the particles inside the accumulation are either in contact with the surfaces of the channel and/or with other particles.[40]

The impact of the particle deposition on the pore surface seems to have less effect on the evolution of ϕ, for pores having a more rectangular section, even though the area of the cross section remains the same as in the square pore case. Indeed, from W around $1.5H$ there is an abrupt increase of ϕ from 0.4 to 0.6 (Fig. 2(b)). In the second and higher range of ϕ within the accumulation, all the cross sections of the channel are

rectangular, with a wider than taller shape and we have various confinements along the height of the channels. Here, the greatest and the smallest mean value of ϕ are around 0.63 and 0.53, respectively, found for almost the same ratio $W/H = 3.2$–3.4 but corresponding to different confinements along the height with $H = 3.4D$ and $H = 4.9D$, respectively. For such high volume fractions we may suppose that the repartition of the particles across the height has to be more homogeneous than in the first ϕ regime even though the structure of the accumulation remains heterogeneous, likely with void regions of various sizes as discussed later. To understand such an increase of ϕ in the 2nd regime, for which the cross section of the channels are rectangular, we focus on channels with the highest confinement along the height, $H = 3.4D$, while it becomes negligible along the channel width ($W = 16.7D$). We

observe a high variability in the structure of the accumulation from one experiment to another. Over a total of twelve identical experiments, the structure of ten of them is globally amorphous while for the other two most of the accumulation exhibits a crystalline-like structure. In the following, we determine how the dynamics of particles accumulation can lead to these two different structures. Fig. 3 reports the evolution of the flow conditions, thanks to the particle velocity, during pore clogging and the subsequent accumulation for two trials performed under the same conditions. In both cases the variation of the mean particle velocity over time, corresponding to the flow decline, is almost identical (Fig. 3(A)) even though the way the channel is initially obstructed is not the same, (Fig. 3(B)) nor are the structures of the subsequent accumulations similar (Fig. 3(C)).
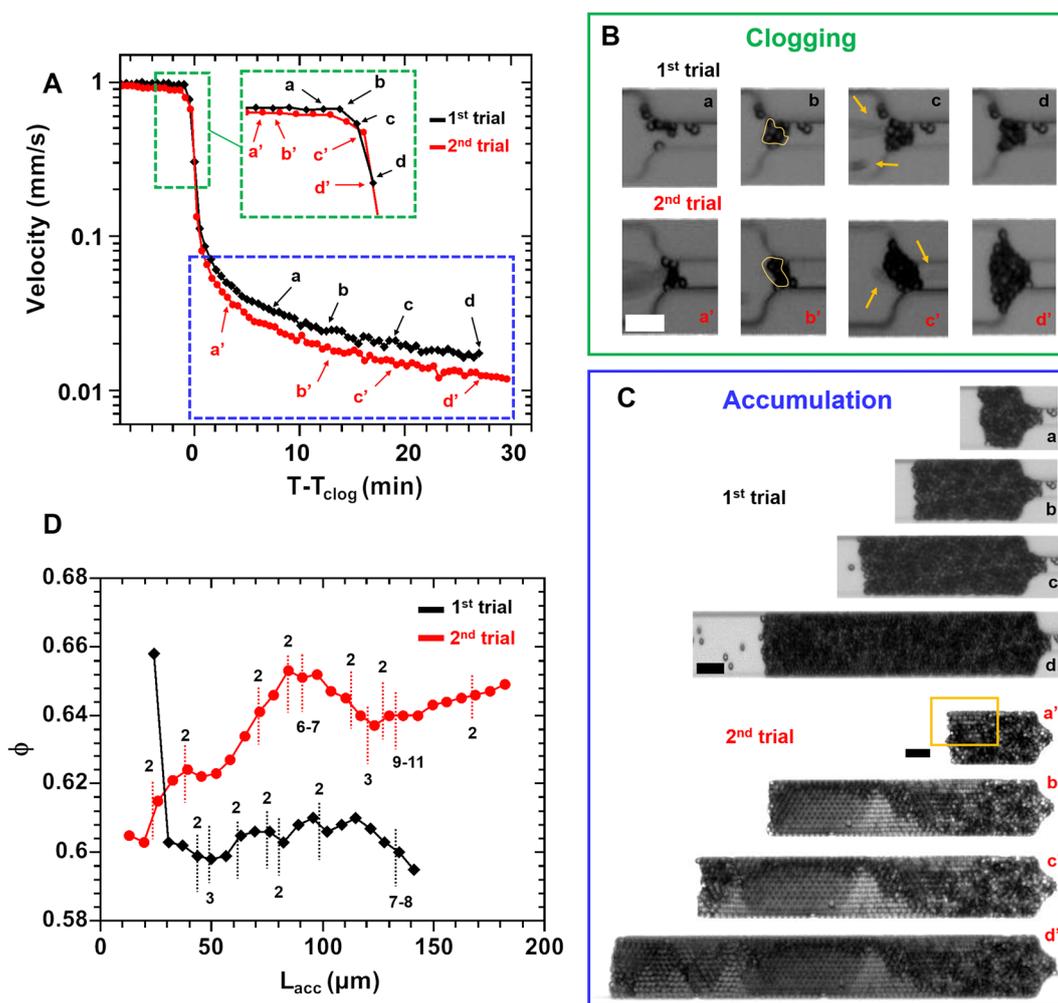
Fig. 3 (A) mean particle velocity *vs.* $T - T_{clog}$, T_{clog} being the time at which the channel is completely obstructed for two trials under the same conditions. The labels within the green (clogging) and blue (accumulation) dashed zones correspond to the image in the top right part in the zones with the same colour, respectively. (B) In the clogging regime we highlight in images b and b′ the biggest aggregates that partakes in the clogs while in images c and c′ the arrows point to particles about to go through the deposit since the pore is not yet completely obstructed. In images d and d′ the two pores are clogged. (C) Consecutive images during the particle accumulation for both trials. The rectangle in image a′ highlights a zone of massive rearrangement which becomes partially ordered without the addition of new particles at the rear of the accumulation (Fig. S3, ESI†). All the scale bars correspond to 10 μm. (D) Variation of the particle volume fraction with the accumulation length for both trials. The arrival of various aggregates corresponds to the dotted lines close to which the number of particles per aggregate is indicated.

There is also a high variability of ϕ with the accumulation length, L_{acc}, between the two trials, as shown in Fig. 3(D). For the 1st trial, from the beginning of the accumulation, ϕ is high, around 60%, and does not significantly change during the growth of the accumulation whose structure is amorphous (Fig. 3(D)). In the other case, the beginning of the accumulation is about the same with an amorphous structure over the first thirty microns (Fig. 3(C), image a′). However, quite rapidly, important spatial rearrangements at the channel surface result in an increase of ϕ, (Fig. 3(C), zone highlighted in image a′). These spatial rearrangements correspond to local transitions from amorphous structures to crystalline ones which are always located at the front of the clog. These crystal structures can also grow over time as new particles arrive and order at this location. The regular arrival of aggregates could explain why the structure of the accumulation of the 1st trial is amorphous and that of the 2nd is not perfectly ordered. Indeed, such particles act as defects, not allowing others to order. However, for both trials, almost the same number of aggregates, 10 or 11, regularly arrives throughout the accumulation, without any noticeable modification of ϕ, even for large aggregates (Fig. 3(D)). This result is not so surprising since we measure the volume fraction over 7 μm, which corresponds to the accumulation of 147 and 161 single particles for the 1st and the 2nd trial, respectively. Therefore, the local modification of the packing due to the presence of an aggregate is completely smoothed out in Fig. 3(D). This also means that even though large aggregates can be viewed as defects they disturb the local order only over a few microns.

Let us look at the accumulation dynamics to elucidate what is responsible for the difference in variation of ϕ for the two trials. For both trials, particle rearrangement events are located at the accumulation front. These events always start at this location, where particles can more easily move, and spread over a limited distance inside the accumulation, L_{event}, with a width smaller than that of the channel. The average value of L_{event} is equal to 6 μm for both trials (Fig. 4(a)), the corresponding average number of particles involved in an event being around 7–8 particles for both trials (Fig. 4(b)). The real number of involved particles is surely greater because we only consider particles in contact with one horizontal surface of the channel and other particles in the vicinity of this moving monolayer are also likely to partake in the rearrangements. Since we are very confined along the height it is also conceivable that a rearrangement could include particles across the entire channel height. Therefore, it would not be surprising that the real number of involved particles in a rearrangement is two to three times higher than what we measure. Note that we have never detected any collective motion well inside the accumulation that is not in contact with the front. This means that there is only local compaction over a few particles layers at the accumulation front throughout the piling up process. Since we work at high Péclet numbers, particles first follow the fluid streamlines until they get arrested at the front. Rapidly after that, other particles that arrive at the front and also the permeation flow push the former particles in such a way that we end up with a more compact structure near the front. For both trials the frequency of

the rearrangements as particle accumulate is important. There is a rearrangement event at the front once 31.5 or 46 particles on average accumulate at the front over a length equals to 1.5 and 2 μm for the 1st and the 2nd trial, respectively.

The number of particles that partakes in such a collective motion fluctuates in a similar manner during the growth of the accumulation in both cases (Fig. 4(d) and (e)). Most of the time several rearrangements take place, one after another, while the accumulation has grown less than a micron. Less frequently, there can be an increase in the accumulation of several microns before seeing another event (Fig. 4(c)–(e)). There is no particular trend for the 1st trial, rearrangements successively occurring irrespectively of their size as particles pile up (Fig. 4(d)). For the 2nd trial, there are larger zones of the accumulation, larger than 40–50 μm, over which the size of the rearrangements are small and similar (rectangles in Fig. 4(e)), followed by a massive collective reorganization spreading over L_{event} between 20 and 30 μm (square symbols in Fig. 4(e)). There are first multiple limited ordering of small assemblies that later merge together in a larger crystalline phase. This suggests that (i) most of the particles are not stuck on the surfaces and thus are free to rearrange at the bottom and top surfaces to form ordered zones, and (ii) particle ordering starts at the surface of the channel as is commonly observed near a flat surface. However, the large crystalline zones are not defect-free with some of these defects being immobile particles in contact with one channel surface. We suppose that if the density of these immobile particles is high enough the structure of the entire clog remains amorphous, as for the 1st trial where there is no local crystallization even though the value of ϕ remains high. This absence of order does not mean that the accumulation is cohesive in the 1st trial since all the particles, except those attached to the walls, leave the clog individually during flow reversal (Movie S1, ESI†).

The role of the immobile particles on the channel surfaces is confirmed by the inspection of the spatial repartition of the particles stuck on the surface (Fig. 5(a) and (b)). We obtain this spatial mapping of the particle immobilized during the clog growth by performing very slow de-clogging experiments, reversing the pressure by imposing a ramp (see Methods). Note that the number of particles that adhere to surfaces during the accumulation may be slightly overestimated since some of them may come into contact with the surfaces during the de-clogging step. We clearly see that there are more particles deposited on the channel surfaces for the less ordered trial (Fig. 5(a) and (b)). We found that there is a cohesive part of the remaining accumulations from which no particle is removed, with a length called hereafter L_{coh}, and next to this there is a zone in which particles are only deposited on the channel surfaces, over a length called L_{dep} (Fig. 5(a) and (b)). We arbitrarily decide that at the end of the zone corresponding to L_{dep} there are less than ten particles on the channel surfaces over the last 10 μm, these particles being not only stuck on the edges but also on the two horizontal surfaces. Note, that after de-clogging, for all the experiments in average $L_{dep} \sim 0.5 L_{tot}$, with L_{tot} the average total length of the accumulation just before the flow reversal (Fig. 5(d)). The influence of particles attached on the channel
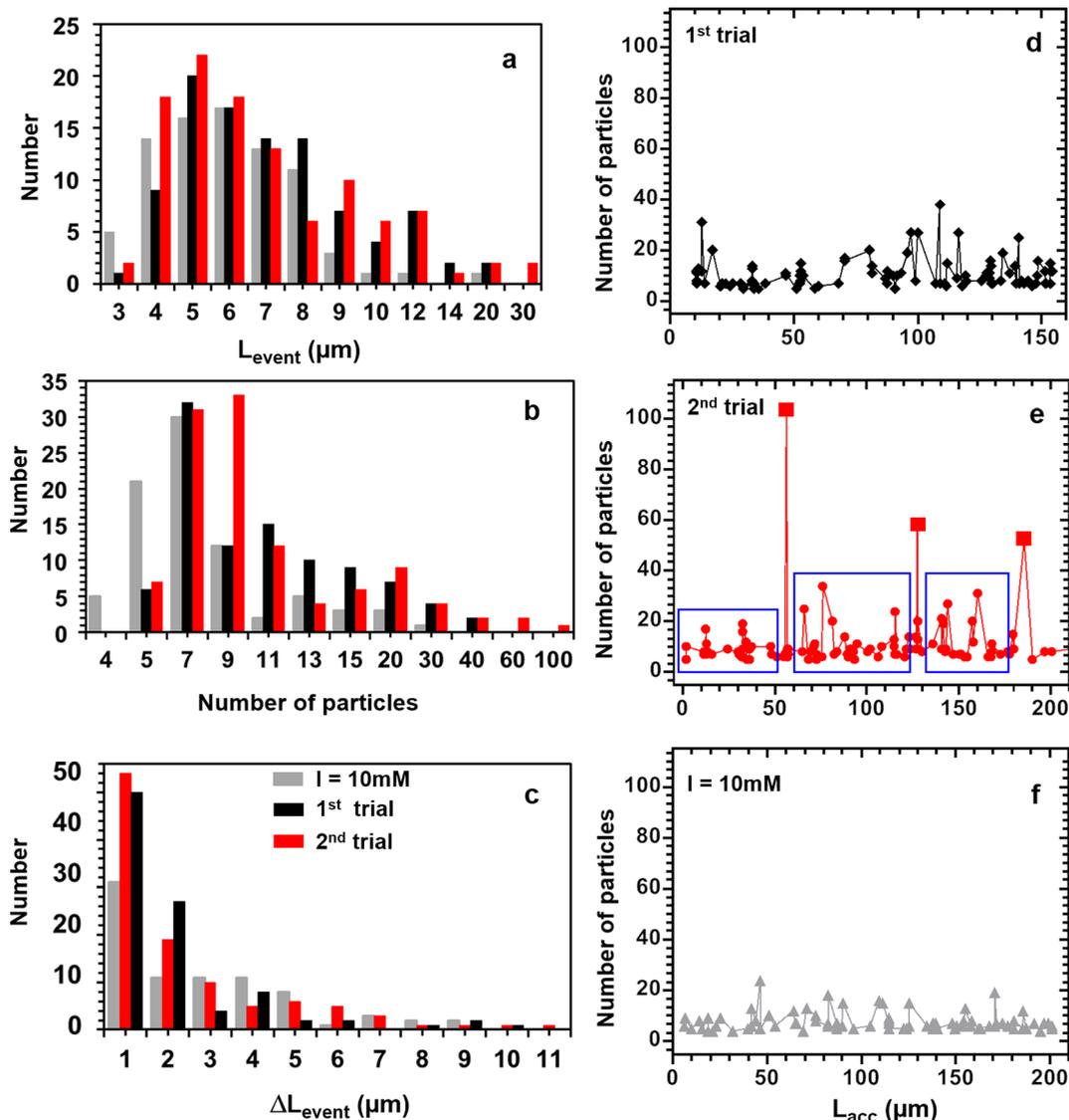
Fig. 4 (a) Distribution of L_{event} with an average value equals to 7.6 μm for both trials and 6.5 for I = 10 mM. (b) Distribution of the distance between two consecutive rearrangement events, ΔL_{event}. (c) Distribution of the number of particles involved in an event. Variation of the number of particles involved in rearrangement events throughout the accumulation, for the 1st trial (d), the 2nd (e) and for I = 10 mM (f). In (e) the zones within the blue rectangles, in which the rearrangement events are small, always precede a more massive amorphous to order transition (three square symbols).

surface, still in this most confined case, can also be studied by modifying the ionic strength, I, of the suspensions. When clogs are formed with $I \geq 1$ mM there is a significant decrease of ϕ from 0.63 down to 0.56 on average, irrespective of the value of I (Fig. 6(a)). This suggest that more particles are stuck on the channel surface for such I values preventing the formation of large crystalline zones leading to larger ϕ values. The way particles pile up and the compaction at the accumulation front for an ionic strength of 1 mM are identical to the no salt case (Fig. 5(c)), with a somewhat lower value of L_{event} (Fig. S5, ESI†). Most of the accumulation is also removed during de-clogging with a slightly greater L_{dep} (Fig. 5(d)). For a higher ionic strength, I = 10 mM, just below the value where the surface charge of the PDMS walls is completely screened (around 30 mM[54]) but still far from the critical coagulation concentration

(CCC) of the suspension (around 150 mM) even more particles are stuck on the channel surfaces (Fig. S4, ESI†) with an noticeable increase of L_{dep} that is a bit smaller than L_{tot} (Fig. 5(d)). Here, the dynamics of compaction are similar to that discussed previously with an alternation of burst of rearrangements that are further from each other (Fig. 4(f)). Rearrangements are also less numerous than in the no salt case (Fig. 4(c)). The mean value of L_{event} keeps slightly diminishing, mainly because there are much less large rearrangements (Fig. 4(a)) with less particles involved in each (Fig. 4(b)). Indeed, due to the greater number of immobile particles on the surfaces there are fewer large rearrangements, which also involve less particles.

When the surface charge of the PDMS walls is completely screened, for I = 50 and 100 mM, there is no compaction
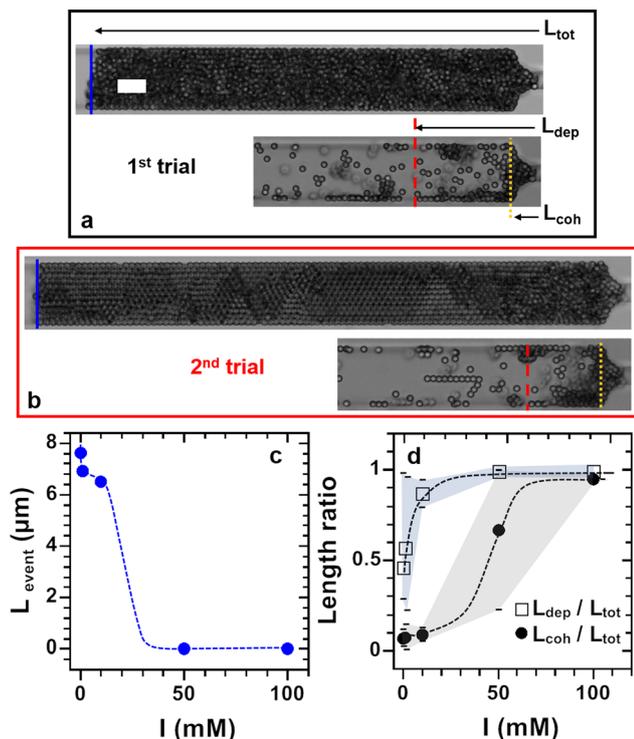
Fig. 5 De-clogging experiments for the no salt case (a and b), corresponding to the two experiments in Fig. 2. In each case the top image is the last one before the flow reversal takes place while the bottom image corresponds to the image of the clog when the de-clog experiment is over. Scale bar is 10 μm. Variation of L_{event} (c) and the ratios of lengths (d) with the ionic strength, the definition of each length being provided in (a). Dashed lines are guides for the eyes and the shaded areas connect the extrema (dashes) of all the data points.

anymore at the accumulation front (Fig. 5(c)). It suggests that as particles pile up on the channel surfaces they get directly stuck there and prevent large collective motions between the two monolayers on these horizontal surfaces. The channel surfaces are covered by monolayers of particles all along the accumulation since $L_{dep}/L_{tot} = 1$ with two-thirds of the accumulation on average not moving during the de-clogging experiments for $I = 50$ mM (Fig. 5(d), and Fig. S4, ESI†). The monolayers in the remaining one-third, are not able to retain the particles on top of them and these individually leave the accumulation (Fig. S4, ESI†). For $I = 100$ mM almost all particles remains in the accumulation (Fig. 5(d)). The greater cohesion of the accumulation in this case is likely due to the large presence of aggregates that represent 10% of the particle of the feeding suspension (Sup. Table, ESI†). Aggregates may have some of their edges stuck on the channel surfaces while others occupy space more in the bulk and these likely prevent movement of individual particles along the flow direction during flow reversal. This is in stark contrast to the no salt case, for which there is first a plug flow of the whole clog with local and temporary formation of crystal zones (Movie S2, ESI†). All the particles end up leaving the channel one after the other, indicating that the accumulation is a dense suspension of repulsive hard spheres on the

overall channel height and length, only held together by the fluid flow.

2 Flow conditions inside the particle accumulation

The local structure of the particle accumulation do not modify the flow conditions across the accumulation for suspensions without salt in the most confined situation (Fig. 3(a) and (d)). Interestingly, despite the noticeable decrease of ϕ between the no salt case and the suspensions with various amounts of added salt, (Fig. 6(a)), the flow decline as the accumulation grows is identical for all these suspensions, as long as I is smaller than the critical coagulation concentration (CCC) of the suspension which is equal to 150 mM (Fig. 6(b)). There is a Darcy flow through the accumulation, except close to the clog head, irrespective of the salinity since the particle velocity varies as the inverse of L_{acc}.[44] Indeed, we found that the permeability, K, is constant all along the accumulation and is the same for all the suspensions (Fig. 6(c)). Therefore, there is no variation of the permeability for all the suspensions, nor a dependence of the permeability with ϕ, as it is generally the case for flow through porous media composed of spherical particles and clogs formed in less confined conditions.[46] Knowing the particle volume fraction helps us to estimate the variation of the permeability along the accumulation using the classical Carman–Kozeny model:[46,55]

$$K = D^2(1 - \phi)^3/A\phi^2,$$

with A is a constant equal to 180.

The comparison with our experimental data reported in Fig. 6(c) and (f) indicates that the Carman–Kozeny relation fails to describe the permeability of our porous media made of colloidal particles. The theoretical permeability value is 4–5 times smaller than the experimentally determined one for $W/D = 3.6$ while it is around twice higher for $W/D = 4.9$. There are several reasons that can explain this failure. Firstly, the flow is too confined, i.e. the number of particle layers along the channel height is too small to neglect the contribution of the flow near the channel surface.[56–59] Secondly, because of the heterogeneous microstructure[60,61] of the accumulation with the presence of void zones,[44,57,62] which inevitably favours an heterogeneous flow through the porous structure. We also observed that when we get closer to the CCC, at $I = 100$ mM, the value of ϕ remains unchanged (Fig. 6(a)) though the permeability is 2–2.5 times greater than for the other suspensions and slightly fluctuates along the accumulation (Fig. 6(c)). To explain such a variation of the flow conditions we recollect that the feeding suspension contains 10% of aggregates, mainly doublets and triplets but also larger objects (Sup. Table, left, ESI†), formed by the coagulation process during the particle synthesis.[42] As mentioned previously, the deposition of aggregates precludes local high compaction of the particles around them, even though we obtain the same ϕ value as seen in other suspensions with less added salt. More importantly the higher concentration of aggregates modifies the permeability all along the accumulation. Indeed, an aggregate larger than quadruplet, with a length equal to the channel height or larger is present
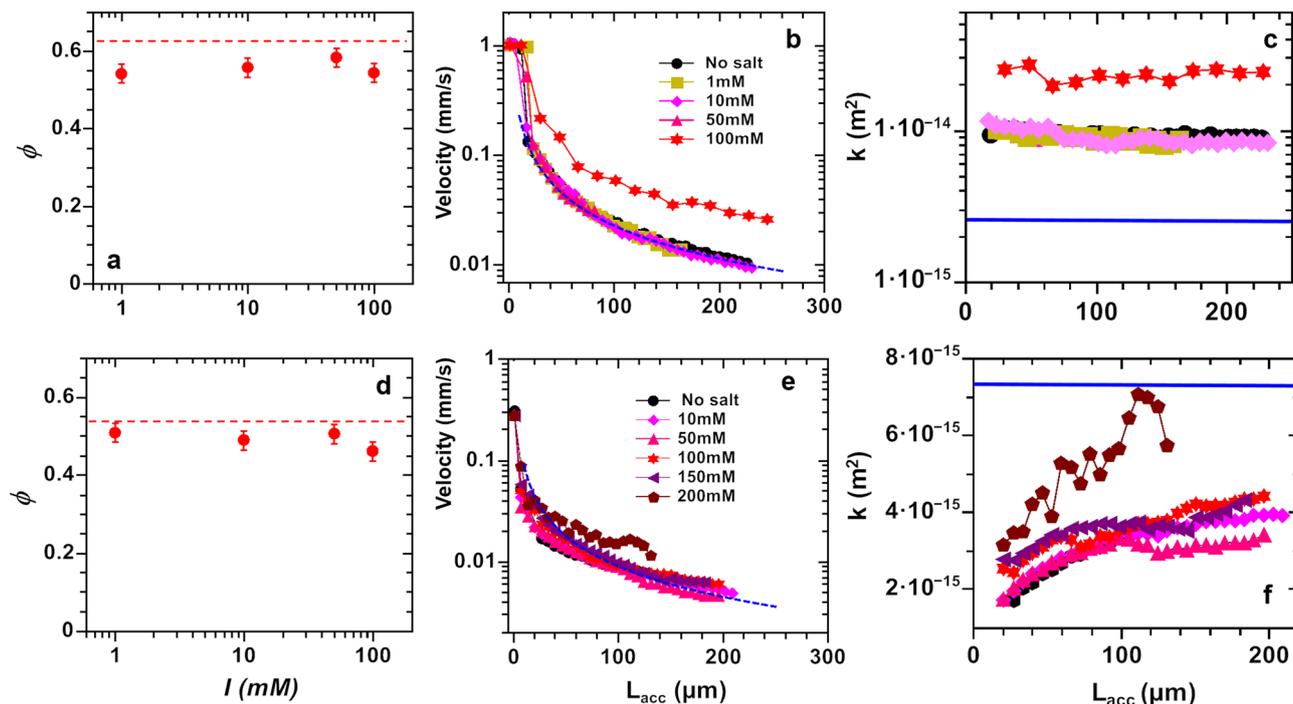
Fig. 6 Variation of the volume fraction inside the accumulation for 2 µm (a) and 1.8 µm PS particles (d) for various ionic strength, inside channel with cross sections ($H \times W$) of 6.9 µm × 21.6 µm and 8.9 µm × 30 µm, respectively. The dashed lines in graphs a and d correspond respectively to ϕ = 0.64 and ϕ = 0.52 for the no salt case. Evolution of the mean particle velocity along the accumulation length for various I conditions for 2 µm (b) and 1.8 µm PS particles (e). The first twenty microns correspond to the clog formation and the dashed lines are inverse power law fits of the data corresponding to Darcy's law. Variation of the corresponding permeability with L_{acc} for 2 µm (c) and 1.8 µm PS particles (f). The blue lines in graphs (c and f) are the permeability according to the Carman−Kozeny model with ϕ = 0.64 and ϕ = 0.52. The graphs of the top and the bottom rows were respectively obtained from the same experiments performed with 2 µm and 1.8 µm PS particle.

inside the particle accumulation every 10–15 µm on average, while for triplets and doublets it is every 5 µm and 1 µm, respectively (Sup. Table, left, ESI†). Hence, the stacking dynamics of this mixture of single particles and aggregates enables the formation of larger pores between particles than those formed solely with single particles. This heterogeneity in the pore size distribution likely favors the emergence of low resistance preferential flow paths that spread all along the accumulation, as observed previously in the same confinement.[44] Another assumption could be that the average pore size is shifted towards a higher value leading naturally to a lower hydrodynamic resistance. In both cases, due to the high salt content, single particles or aggregates as they enter in the accumulation can easily adhere irreversibly to others, further preventing rearrangements inside the accumulation by fluid compaction at its front and thus, this favors the presence of larger pores.

For a lower confinement along the channel height, using 1.8 µm PS particles in a 8.9 µm high channel, we obtain a systematically smaller ϕ value in the no salt case than seen previously, corresponding to a very loose random packing of the particles inside the accumulations, $\phi \approx 0.52$ (Fig. 6(d)). We also observed local crystallization which suggests that this ordering process is limited to the monolayers in contact with the horizontal surfaces of the channel. Indeed, the diffusion is more effective at ordering the particles close to the channel surfaces since the flow is very low or negligible compared to the

Brownian motion of the particles. There is almost no variation of ϕ when salt is added to the suspension, which further indicates that organization of the particles at the surfaces does not completely pilot the variation of ϕ as in the case of the high confinement regime (Fig. 6(d)). We observe a slight but noticeable decrease of ϕ when we get closer to the CCC (200 mM) of the suspension, for I = 150 mM. The number of aggregates rises up and reaches 13.6% of the particle population (Table S1, right, ESI†). For this lower confinement we get a similar variation of the permeation flow through the accumulation for all the suspensions except, again, when we come closer to the CCC. There is a slower Darcy flow with a slight but noticeable increase of the permeability over the first 60 µm before becoming constant (Fig. 6(f)). Closer to the CCC, for I = 200 mM it becomes difficult to measure the value of ϕ, but we can still determine that aggregates now represent 76% of the particle population of the feeding suspension, half of them being as big as quadruplets (Sup. Table, right, ESI†). As in the more confined situation, the permeability is higher than for the other suspensions, twice as high on average (Fig. 6(f)). This is expected since the particle packing is highly disordered with a mean pore size greater than that obtained for accumulations mostly formed from single particles. This is due to the even higher polydispersity of the various objects that accumulate, which thus explain the greater value of the mean permeability along the accumulation. In addition, the cohesion between

particles and the irreversible adhesion on the channel surfaces prevent local compaction within the bulk of the accumulation and hence the decrease in the mean pore size as particles pile up. During particle stacking preferential flow paths, which connect void zones, may also have been created, which also contributes to the increase of the clog permeability.[44]

3 Influence of flow intensity on particle accumulation

The variation of flow conditions is another parameter that could influence the structure of the accumulation of particles and the flow through it. We changed the applied pressure such that the initial flow rate was varied over half a decade and did not see any noticeable evolution of ϕ in the highest confinement, for $H/D = 3.4$ (Fig. 7(a)). The flow declines corresponding to the formation of the clog head are similar but are not exactly the same for each pressure,[44] (Fig. 7(b)), while there is significant variations of the permeability of the accumulation, with no specific trend with the pressure (Fig. 7(c)). In some cases K does not change with L_{acc} (5–10 and 20 mbar) while for others it first increases with L_{acc} and then becomes constant (7–12 and 15 mbar). K increases by a factor 2.5 between the lowest and the highest permeability. Such a K variation was previously observed for the same confinement along the height, when we compare an accumulation formed with a negligible number of aggregates with another one containing 10% aggregates (Fig. 6(c)). This suggests that varying the applied pressure can modify the preferential flow paths within the accumulation without noticeably changing the ϕ value, even though the

suspensions we used contain a small number of aggregates. To explain such variations of K we suppose that there is either a compaction of the accumulation or a fluctuating number of particles that are in contact with the channel surfaces. While rearrangements that occur over 7 μm close to the accumulation front leads to a continuous but localized compaction for the lowest pressure of 5 mbar (Fig. 4(a)), it is not the case neither at the front nor elsewhere inside the accumulation for all the other higher pressures. This indicates that there is no compaction or noticeable rearrangement within the accumulation when we increase the applied pressure. To test the second hypothesis concerning the potential role played by the particles attached on the channel surface we performed de-clogging experiments for particle accumulations obtained with various applied pressures. As before, we consider the evolution of the two length ratios, L_{dep}/L_{tot} and L_{coh}/L_{tot} with the pressure (Fig. 7(d)). For the lowest pressure almost all the particles inside the accumulation leave the channel during the flow reversal (Fig. 5(a)). At the end of this process the remaining part of the particle accumulation is small and roughly equal to 10 μm on average. Actually, this part likely corresponds to the end of clog head and not to the accumulation behind it, and thus cannot be removed by the low flow rate we used for the flow reversal since the clog head is a cohesive assembly. For a slightly higher pressure, equal to 7 mbar, there is a steep increase of the ratio L_{dep}/L_{tot} that reaches 0.8, with a higher density of particles on the channel surfaces (Fig. S5, ESI†), especially in the first thirty microns of the accumulation, on average, corresponding to L_{coh} (Fig. 7(d)). One-third to half of this length belongs to the clog head while the remaining part truly corresponds to the apparent cohesive part of the accumulation. Indeed, we suppose that over L_{coh} particles not directly in contact with the channel surfaces are not stuck to each other since the flow is not high enough to allow such an adhesion.[41,42,44] These particles are mostly retained by those glued on the channel surfaces, forming local arches that prevent their motion during the de-clogging process. This remains true as long as the particle density on the channel surface is high enough, which is not the case anymore further along the accumulation, up to the end of the part of the channel corresponding to L_{dep}. It is difficult to quantify the density of particles on the surfaces needed to retain the others in the bulk with our experiments since particles can also be stuck on the surfaces during the de-clogging process and not just during the particle accumulation. Indeed, during accumulation particles arrive at the front one by one, while when the flow is reversed a dense suspension flows through the channel which leads to an intermittent transport with temporary blockages[63,64] during which particles are pushed towards the walls and thus are forced to adhere to them.

For a pressure larger or equal to 10 mbar the flow intensity is high enough to partially cover the channel surfaces on the overall accumulation since $L_{dep}/L_{tot} = 1$. In addition, 80% up to 95% of the stacked particles do not move during the flow reversal, corresponding to $L_{coh}/L_{tot} > 0.8$ (Fig. 7(d)). Therefore, only the particles close to the accumulation front are able to
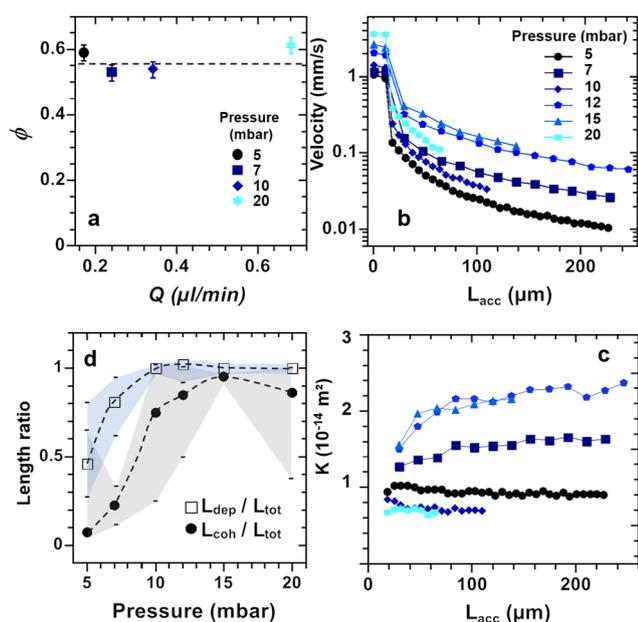

Fig. 7 (a) Variation of the volume fraction inside the accumulation for 2 μm spheres for various pressures. The dashed lines corresponds to the mean ϕ value for all the pressures. (b) Evolution of the mean particle velocity along the accumulation length. (c) Variation of the permeability K along L_{acc}, obtained from the data of graph (b) (d) Variation of the ratios of lengths with the pressure. Dashed lines are guides for the eyes and the shaded areas connect the extrema (dashes) of all the data points.
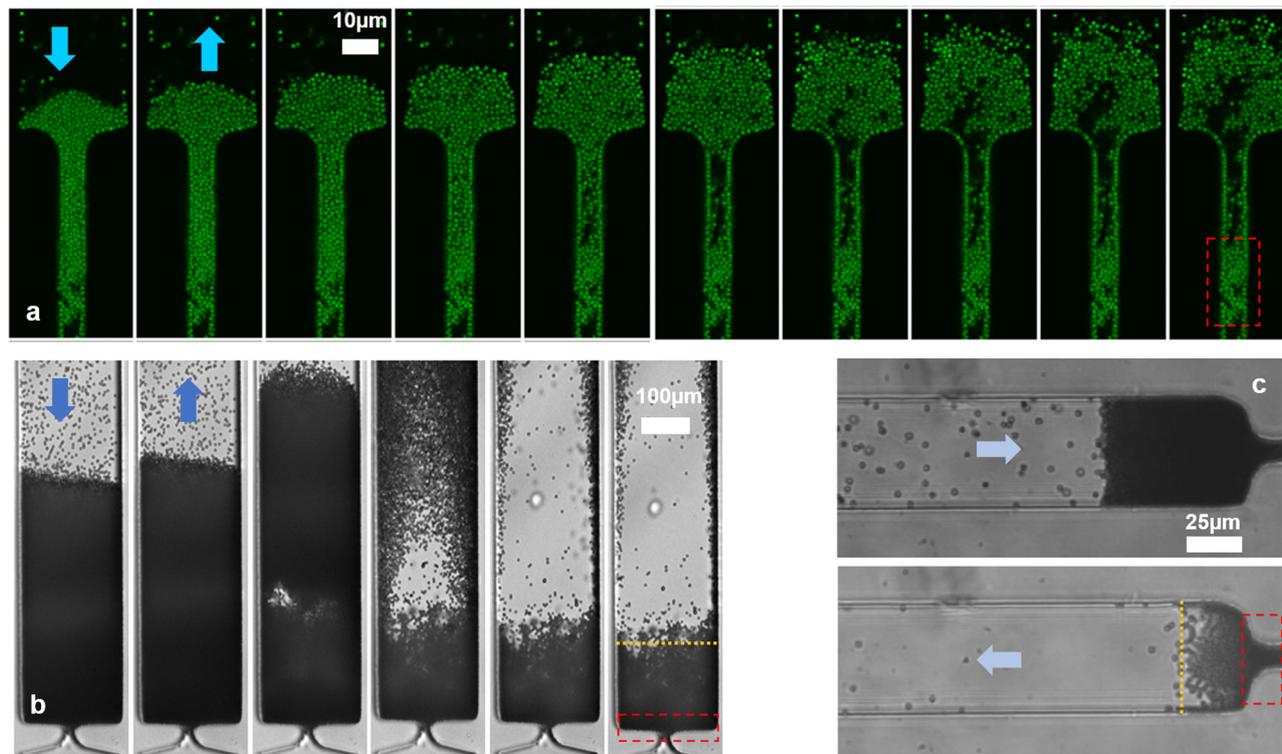
Fig. 8 (a) Confocal images of a de-clogging experiments for 1.8 μm PMMA particles inside a channel with $H = 11$ μm and $W = 9$ μm. The particle accumulation was formed at 30 mbar (1st image on the left) and we zero the pressure thereafter, from the 2nd image up to the last one on the right. We focus at the middle height of the channel to show that there is no particle in the bulk after de-clogging. De-clogging of a single channel filled with 4 μm PS at 35 mbar (b) or 2 μm PS at 10 mbar (c) inside a channel with $H = 50$ and 53 μm and $W = 200$ and 50 μm, respectively. In both cases we also zero the pressure, which leads to flow reversal. Dashed rectangles correspond to the clog head while the dotted lines are the end of the deposition zones of particles on the channel surfaces, as in Fig. S3 and S5 (ESI†). The arrows point to the flow direction.

follow the fluid and leave the accumulation during the flow reversal. We conclude that as the applied pressure increases more particles are stuck on the channel surfaces allowing the extension of the apparent cohesive part of the accumulation. However the density of particles stuck on the surfaces is not the only important parameter, the repartition of the particles one from another on the same surface but also on the opposite surface should also be critical.

We have to keep in mind that the final repartition of particles on both horizontal surfaces is coupled and depends on the specific piling up process encountered as each accumulation grows. This explains why from one trial to another there is a high variability in the particle repartition on the channel surfaces and also in the length of the cohesive part (Fig. S5, ESI†). Note, that whatever the applied pressure is, the zone close to the rear of the accumulation is systematically removed during the flow reversal, indicating that this zone is weaker than the rest of the accumulation. Therefore, we suggest that there is always a final compaction of the accumulation even for the pressures for which no rearrangement event at the front has been detected. This is possible since our event detection is performed only on the channel surfaces and thus compaction of the particles not in contact with the surfaces may occur without being monitored. In this case, the permeation flow pushes the particles in the middle of the channel against those

immobile on the channel surfaces, forming in this way multiple stable arches across the height of the channel, since it is only physically possible to fit three to five particle layers within this height. The situation is a bit different when the accumulation process takes place for higher pressures but in lower confinement over the height of the channel and along its width. We found that all the particles behind clog heads are removed by the flow reversal during de-clogging in various channels, except those in contact with the channel surfaces, close to the clog head (Fig. 8), a phenomenon also observed by Mokrane *et al.*[45] Most of the particles inside the accumulation are in the bulk and form a dense suspension of repulsive spheres, held together by the fluid flow. The concentration of the suspension is such that particles are able to push some of those that are close to the channel surfaces, forcing them to adhere to the surfaces. For lower flow conditions, the amorphous-to-order transition at the channel surfaces should take place since the flow closer to the surface is lower than for the confined case and thus diffusion can enhance particle ordering.[45]

Conclusions

In this paper we determine the variation of the structural features of an accumulation of particles formed consecutively

to the obstruction of a constriction formed by similar colloidal particles. We also determine the permeation flow across this accumulation when we vary the confinement, ionic strength and flow conditions. We first show that the piling dynamics of the particles that compose the accumulation strongly depends on the shape and size of the cross section of the channel and leads to two distinct regimes of particle volume fraction, ϕ. Particle assembly inside channels with a squared cross section has a very low values of ϕ, around 0.3–0.4, while for rectangular channels ϕ values are closer to 0.5–0.6. A high confinement, both along the width and the height of the channel or, only in its larger dimension is responsible for such variations of ϕ, by enhancing the adhesion of particles on the channel surfaces, which in turns dictates the structure of the accumulation further in the bulk. This remains true even for large variations of ionic strength. Since confinement is always not negligible in all our experiments, the structure of the particle accumulations is always quite heterogeneous and thus the knowledge of ϕ is not useful to determine their permeability, with most of the fluid expected to be flowing through preferential paths, along which the local values of particle volume fraction are supposed to be lower than the average ϕ value. When I becomes close to the CCC of the colloidal suspension there is a large polydispersity in the aggregates that compose the particle accumulation. This leads to a higher permeability of the accumulation when compared to those formed with lower I, irrespective of the confinement dimensions.

Finally we demonstrate that the nature of the clog and the particle accumulation behind it are not the same. The accumulation is a dense assembly of repulsive spheres as long as the particle are stable against aggregation, irrespective of the investigated flow conditions, while the particles within the clog adhere on to each other, forming a cohesive assembly. Therefore, during a flow reversal the particle accumulation can easily be removed from the clog as long as the confinement is not too important.

Further, similar, studies may be performed using greater cross section channels, for which particles deposited on the channel surfaces should have a negligible impact on the structural features on the dense assembly of repulsive particles in the bulk. In such a case the compaction may be not located only at the accumulation front. Indeed, since there are variations of the fluid velocity across the channels we may expect that there could also be local variations of ϕ within the accumulation. In other words, the repartition of the permeation flow through the accumulation may modify the local compaction. It would be interesting to study if particle rearrangements can allow a local transition from an amorphous packing to a crystalline one and how this affects the overall accumulation. From a practical point of view, even though the geometry of the channel we used is a bit peculiar, we think that our results may help understand some of the physical processes at play inside the pores of the filters or membranes fouled by colloidal particles.

Conflicts of interest

There are no conflicts of interest to declare.

Acknowledgements

References

1 R. D. Deegan, O. Bakajin, T. F. Dupont, G. Huber, S. R. Nagel and T. A. Witten, *Nature*, 1997, **389**, 827–829.

2 A. Rushton, A. S. Ward and R. G. Holdich, *Solid-Liquid Filtration and Separation Technology*, John Wiley & Sons, 2008.

3 M. R. Mackley and N. E. Sherman, *Chem. Eng. Sci.*, 1992, **47**, 3067–3084.

4 J. Emile and H. Tabuteau, *Colloids Surf., A*, 2016, **511**, 201–211.

5 L. Li, C. Goodrich, H. Yang, K. R. Phillips, Z. Jia, H. Chen, L. Wang, J. Zhong, A. Liu, J. Lu, J. Shuai, M. P. Brenner, F. Spaepen and J. Aizenberg, *Proc. Natl. Acad. Sci. U. S. A.*, 2021, **118**(32), e2107588118.

6 R. Piazza, S. Buzzaccaro, E. Secchi and A. Parola, *Soft Matter*, 2012, **8**, 7112–7115.

7 C. R. Nugent, K. V. Edmond, H. N. Patel and E. R. Weeks, *Phys. Rev. Lett.*, 2007, **99**, 025702.

8 P. Scheidler, W. Kob and K. Binder, *Europhys. Lett.*, 2002, **59**, 701.

9 G. L. Hunter, K. V. Edmond and E. R. Weeks, *Phys. Rev. Lett.*, 2014, **112**, 218302.

10 R. C. Roberts, N. Marioni, J. C. Palmer and J. C. Conrad, *Mol. Phys.*, 2020, **118**, e1728407.

11 M. Spannuth and J. C. Conrad, *Phys. Rev. Lett.*, 2012, **109**, 028301.

12 K. V. Edmond, C. R. Nugent and E. R. Weeks, *Eur. Phys. J.-Spec. Top.*, 2010, **189**, 83–93.

13 H. B. Eral, D. van den Ende, F. Mugele and M. H. G. Duits, *Phys. Rev. E: Stat., Nonlinear, Soft Matter Phys.*, 2009, **80**, 061403.

14 P. S. Sarangapani and Y. Zhu, *Phys. Rev. E: Stat., Nonlinear, Soft Matter Phys.*, 2008, **77**, 010501.

15 A. Villada-Balbuena, G. Jung, A. B. Zuccolotto-Bernez, T. Franosch and S. U. Egelhaaf, *Soft Matter*, 2022, **18**, 4699–4714.

16 P. Pieranski, L. Strzelecki and B. Pansu, *Phys. Rev. Lett.*, 1983, **50**, 900–903.

17 B. Pansu, P. Pieranski and P. Pieranski, *J. Phys.*, 1984, **45**, 331–339.

18 S. Neser, C. Bechinger, P. Leiderer and T. Palberg, *Phys. Rev. Lett.*, 1997, **79**, 2348–2351.

19 A. Fortini and M. Dijkstra, *J. Phys.: Condens. Matter*, 2006, **18**, L371–L378.

20 C. P. Ortiz, R. Riehn and K. E. Daniels, *Soft Matter*, 2012, **9**, 543–549.

21 C. P. Ortiz, K. E. Daniels and R. Riehn, *Phys. Rev. E: Stat., Nonlinear, Soft Matter Phys.*, 2014, **90**, 022304.

22 C. P. Ortiz, R. Riehn and K. E. Daniels, *J. Stat. Mech.*, 2016, **2016**, 084003.

23 S. Lin and M. R. Wiesner, *Environ. Sci. Technol.*, 2012, **46**, 13270–13277.

24 M. R. de Saint Vincent, M. Abkarian and H. Tabuteau, *Soft Matter*, 2016, **12**, 1041–1050.

25 E. Dressaire and A. Sauret, *Soft Matter*, 2017, **13**, 37–48.

26 D. C. Mays, *J. Environ. Eng.*, 2010, **136**, 475–480.

27 C. Duchêne, V. Filipe, S. Huille and A. Lindner, *Soft Matter*, 2020, **16**, 921–928.

28 B. Mustin and B. Stoeber, *Microfluid. Nanofluid.*, 2010, **9**, 905–913.

29 A. Sauret, E. C. Barney, A. Perro, E. Villermaux, H. A. Stone and E. Dressaire, *Appl. Phys. Lett.*, 2014, **105**, 074101.

30 S. Pan, J. M. G. Tzoc Torres, T. Hoare and R. Ghosh, *J. Membr. Sci.*, 2015, **479**, 141–147.

31 I. Bouhid de Aguiar, M. Meireles, A. Bouchoux and K. Schroën, *Sci. Rep.*, 2019, **9**, 9241.

32 V. Ramachandran and H. S. Fogler, *J. Fluid Mech.*, 1999, **385**, 129–156.

33 G. C. Agbangla, É. Climent and P. Bacchin, *Sep. Purif. Technol.*, 2012, **101**, 42–48.

34 G. C. Agbangla, E. Climent and P. Bacchin, *Comput. Fluids*, 2014, **94**, 69–83.

35 M. Souzy, I. Zuriguel and A. Marin, *Phys. Rev. E*, 2020, **101**, 060901.

36 A. Marin, H. Lhuissier, M. Rossi and C. J. Kähler, *Phys. Rev. E*, 2018, **97**, 021102.

37 G. Constant Agbangla, P. Bacchin and E. Climent, *Soft Matter*, 2014, **10**, 6303–6315.

38 N. Vani, S. Escudier and A. Sauret, *Soft Matter*, 2022, **18**, 6987–6997.

39 B. Dersoir, M. R. de, S. Vincent, M. Abkarian and H. Tabuteau, *Microfluid. Nanofluid.*, 2015, **19**, 953–961.

40 B. Dersoir, A. B. Schofield, M. Robert de Saint Vincent and H. Tabuteau, *J. Membr. Sci.*, 2019, **573**, 411–424.

41 N. Delouche, J. M. van Doorn, T. E. Kodger, A. B. Schofield, J. Sprakel and H. Tabuteau, *J. Membr. Sci.*, 2021, **635**, 119509.

42 N. Delouche, A. B. Schofield and H. Tabuteau, *Soft Matter*, 2020, **16**, 9899–9907.

43 B. Dersoir, A. B. Schofield and H. Tabuteau, *Soft Matter*, 2017, **13**, 2054–2066.

44 N. Delouche, B. Dersoir, A. B. Schofield and H. Tabuteau, *Phys. Rev. Fluids*, 2022, **7**, 034304.

45 M. Larbi Mokrane, T. Desclaux, J. F. Morris, P. Joseph and O. Liot, *Soft Matter*, 2020, **16**, 9726–9737.

46 A. Sauret, K. Somszor, E. Villermaux and E. Dressaire, *Phys. Rev. Fluids*, 2018, **3**, 104301.

47 S. Shen, E. D. Sudol and M. S. El-Aasser, *J. Polym. Sci., Part A: Polym. Chem.*, 1993, **31**, 1393–1402.

48 T. E. Kodger, R. E. Guerra and J. Sprakel, *Sci. Rep.*, 2015, **5**, 14635.

49 A. Lüken, L. Stüwe, J. Lohaus, J. Linkhorst and M. Wessling, *Sci. Rep.*, 2021, **11**, 12836.

50 B. Dincau, C. Tang, E. Dressaire and A. Sauret, *Soft Matter*, 2022, **18**, 1767–1778.

51 A. D. Dinsmore and D. A. Weitz, *J. Phys.: Condens. Matter*, 2002, **14**, 7581–7597.

52 V. Trappe, V. Prasad, L. Cipelletti, P. N. Segre and D. A. Weitz, *Nature*, 2001, **411**, 772–775.

53 A. I. Campbell, V. J. Anderson, J. S. van Duijneveldt and P. Bartlett, *Phys. Rev. Lett.*, 2005, **94**, 208301.

54 B. Mustin and B. Stoeber, *Langmuir*, 2016, **32**, 88–101.

55 J. Bear, *Dynamics of Fluids in Porous Media*, Courier Corporation, 1988.

56 B. Eisfeld and K. Schnitzlein, *Chem. Eng. Sci.*, 2001, **56**, 4321–4329.

57 R. F. Benenati and C. B. Brosilow, *AIChE J.*, 1962, **8**, 359–361.

58 P. M. Bandelt Riess, H. Briesen and D. Schiochet Nasato, *Granular Matter*, 2022, **24**, 36.

59 S. Ehlert, T. Rösler and U. Tallarek, *J. Sep. Sci.*, 2008, **31**, 1719–1728.

60 M. a V. D. Hoef, R. Beetstra and J. a M. Kuipers, *J. Fluid Mech.*, 2005, **528**, 233–254.

61 R. M. McDonogh, A. G. Fane, C. J. D. Fell and H.-C. Flemming, *Colloids Surf., A*, 1998, **138**, 231–244.

62 S. Zhang and J. J. McCarthy, *AIChE J.*, 2019, **65**, e16557.

63 L. Isa, R. Besseling, A. N. Morozov and W. C. K. Poon, *Phys. Rev. Lett.*, 2009, **102**, 058302.

64 P. Kanehl and H. Stark, *Phys. Rev. Lett.*, 2017, **119**, 018002.